Mediation of high temperature radiation damage in bcc iron by Au or Cu precipitation

Zhang, Shasha; Yao, Zhengjun; Zhang, Zhaokuan; Oleksandr, Moliar; Chen, Feida; Cao, Xingzhong; Zhang, Peng; van Dijk, Niels; van der Zwaag, Sybrand

DOI
10.1016/j.nimb.2019.11.035

Publication date
2020

Document Version
Final published version

Published in
Nuclear Instruments and Methods in Physics Research, Section B: Beam Interactions with Materials and Atoms

Citation (APA)
Zhang, S., Yao, Z., Zhang, Z., Oleksandr, M., Chen, F., Cao, X., Zhang, P., van Dijk, N., & van der Zwaag, S. (2020). Mediation of high temperature radiation damage in bcc iron by Au or Cu precipitation. *Nuclear Instruments and Methods in Physics Research, Section B: Beam Interactions with Materials and Atoms*, *463*, 69-75. https://doi.org/10.1016/j.nimb.2019.11.035

Nuclear Inst. and Methods in Physics Research B 463 (2020) 69–75

Contents lists available at ScienceDirect

Nuclear Inst. and Methods in Physics Research B

journal homepage: www.elsevier.com/locate/nimb

Mediation of high temperature radiation damage in bcc iron by Au or Cu precipitation

Shasha Zhang[a,b,*], Zhengjun Yao[a,b], Zhaokuan Zhang[a], Moliar Oleksandr[a,b], Feida Chen[a], Xingzhong Cao[c], Peng Zhang[c], Niels van Dijk[d], Sybrand van der Zwaag[e,f]

[a] College of Materials and Technology, Nanjing University of Aeronautics and Astronautics, Nanjing 211106, People's Republic of China
[b] Key Laboratory of Materials Preparation and Protection for Harsh Environment (Nanjing University of Aeronautics and Astronautics), Ministry of Industry and Information Technology, Nanjing 211106, People's Republic of China
[c] Institute of High Energy Physics, Chinese Academy of Sciences, Beijing 100049, China
[d] Fundamental Aspects of Materials and Energy group, Faculty of Applied Sciences, Delft University of Technology, Mekelweg 15, 2629 JB Delft, The Netherlands
[e] Novel Aerospace Materials group, Faculty of Aerospace Engineering, Delft University of Technology, Kluyverweg 1, 2629 HS Delft, The Netherlands
[f] School of Materials Science and Engineering, Tsinghua University, Beijing, People's Republic of China

ARTICLE INFO

Keywords:
Au/Cu precipitation
Radiation damage
Hardening
Positron annihilation spectroscopy
Nanoindentation
bcc Fe

ABSTRACT

High temperature radiation damage in binary bcc Fe alloys containing 1 atomic % Au or Cu due to Fe ion irradiation at 550 °C to a peak dose of 2.8 and 8.3 dpa is studied. The precipitation behavior of gold and copper and its correlation to the irradiation-induced defects is studied by transmission electron microscopy and variable energy positron annihilation spectroscopy (VEPAS). The increase of *S* parameters from VEPAS indicates the formation of open volume defects upon irradiation. Disc-shaped Au precipitates, grown from the irradiation induced dislocations, are observed in the Fe-Au alloy. In the Fe-Cu alloy, spherical Cu particles are formed but no direct connection between Cu precipitates and radiation damage is detected. For the Fe-Au alloy, the surface hardness dramatically increases for a dose of 2.8 dpa, with a slight decrease as the irradiation dose is enhanced to 8.3 dpa. In the Fe-Cu alloy, radiation hardening increases continuously.

1. Introduction

During service in a nuclear reactor, microstructural damage in the form of vacancies, dislocations and cavities is generated in the structural components as a result of the irradiation by neutrons, ions and electrons. The radiation damage can lead to swelling, hardening, amorphization and embrittlement, limiting the lifetime and stability of structural steels in nuclear reactors [1,2]. Earlier work has shown that substitutional solute segregation and precipitation occurs under irradiation in alloys both at room and elevated temperatures [3]. The radiation-induced solute redistribution results in a swelling reduction, which arises from the trapping of points defects by alloying elements [4]. For example, irradiation-induced $Cr_{23}C$ precipitates were found to form at dislocation loops in austenitic stainless steel [5]. Work by Ono and coworkers further revealed the Cr segregation at the He bubble surface in a Fe-9Cr% steel [6].

Copper, either as an intentionally added alloying element or as an impurity, is a commonly occurring element in steels used for radiation sensitive components near the core of water cooled nuclear reactors. The correlation between the irradiation-induced defects and Cu precipitates has been studied both theoretically [7–9] and experimentally [10–12]. Microstructural studies have shown that the irradiation-induced or enhanced Cu-rich precipitates (CRPs) are responsible for the irradiation hardening in copper-bearing iron-based alloys as they impede the dislocation motion [13–16]. However, most of such radiation induced precipitation studies focused on the evolution of radiation hardening at room temperature. Considering the high temperature service conditions in advanced nuclear reactors (300–800 °C), high temperature irradiation studies on the radiation damage and Cu precipitates with their effect on the microstructure and the mechanical properties are of greater significance. Hardie and coworkers observed the irradiation hardening on self-ion implanted Fe-Cr alloys at temperatures of 300 and 400 °C whereas no hardening was detected after irradiation at 500 °C [17]. Yabuuchi and coworkers studied the dose dependence of irradiation hardening in Fe-1Cu alloys at a temperature of 290 °C and found a significant radiation hardening which saturated when the alloy was irradiated to 0.1 dpa [18].

While Cu is a common and known alloying element it is also very

* Corresponding author.
E-mail address: s.zhang@nuaa.edu.cn (S. Zhang).

https://doi.org/10.1016/j.nimb.2019.11.035
Received 17 October 2019; Received in revised form 18 November 2019; Accepted 20 November 2019

interesting to study the correlation between radiation damage and the precipitation of dissolved Au atoms in ferrous alloys since: (i) copper and gold have about the same solubility in *bcc* Fe; (ii) in contrast to copper precipitation, the strain energy generated during nucleation and growth for Au precipitation is high due to the large size difference between solute and solvent atoms [19]; (iii) *ab-initio* calculations have predicted a strong interaction between solute Au and the irradiation-induced defects [20,21]. In our recent study [22], we investigated the correlation between Au precipitation and defects induced by helium implantation and found the autonomous precipitation on the cavities, demonstrating a high self-healing potential. However, since the He atoms reduce the interaction between Au atoms and defects, the binding between Au precipitates and radiation damage is inhibited. In this study, open-volume defects, i.e., dislocations, are generated. The chemical environment and strain fields of are very different from the He filled cavities. The *ab initio* calculations indicated a close correlation between Au atoms and open-volume defects, which can influence the precipitation behavior and radiation damage evolution and subsequently the hardening behavior. Moreover, a comparison between the precipitation behavior of Au and Cu solutes, which differ principally in their atom sizes (the size factor of Au and Cu in bcc Fe is $\Omega_{sf}^{Cu} = 0.18$ and $\Omega_{sf}^{Au} = 0.44$, respectively [23]), can clarify the effect of solute size factor on the precipitation and its correlation with radiation damage in nuclear structural alloys. The depth dependent radiation hardening phenomena have been studied for both alloys in order to study the mechanical properties evolution under irradiation.

2. Materials and methods

Fe-Au and Fe-Cu model alloys with an addition of around 1 at. % Au and Cu solute atoms were prepared by vacuum arc melting. The compositions of both alloys are shown in Table 1. The Fe–Au and Fe-Cu alloys were solution treated in evacuated and sealed silica tubes filled with ultrahigh-purity argon gas at 868 °C for 5 h and 850 °C for 1 h, respectively, and subsequently quenched into water at room temperature. All the samples are square sheet materials with dimensions of 10 mm × 10 mm × 1 mm. The specimens were first mechanically polished with grade 800–2000 silicon carbide paper and then chemo-mechanically polished using a suspension of colloidal silica (0.04 μm) to a mirror-like surface. For both alloys the average (equiaxed) grain size was found to be 32 ± 3 μm.

Variable energy positron annihilation spectroscopy (VEPAS) measurements were carried out on a slow positron beam with ^{22}Na radiation source (activity of 1.85 GBq). The Doppler Broadening (DB) of the positron annihilation photon peak was measured using a high-purity Ge detector with an energy resolution of 1.3 keV at 511 keV. Two parameters (*S* and *W*) were calculated from the annihilation photo-peak. The *S* and *W* parameters were defined as the ratio of the number of counts in the central energy region (511 ± 0.8 keV) and in two high momentum regions (515.0–519.2 keV and 502.8–507.0 keV) of the annihilation photon peak normalised to the total number of counts in the peak, respectively. VEPAS experiments were performed on unirradiated and irradiated samples.

The specimens were irradiated on the 320 kV-platform at the Institute of Modern Physics, Chinese Academy of Science (CAS). Irradiations were performed using 3 MeV self-ion Fe^{13+} to fluences of 2.66×10^{15} and 7.98×10^{15} ions/cm^2, respectively, at a temperature

Table 1
Chemical composition of the studied Fe-Au and Fe-Cu alloys (in at. %) with balance iron.

Alloy	Au	Cu	C	P	S	Si
Fe-Au	1.23	–	0.010	0.037	0.002	0.051
Fe-Cu	–	1.02	0.034	0.010	< 0.002	0.058

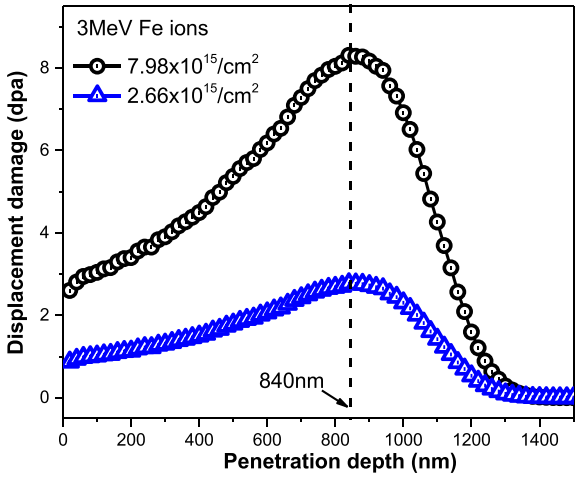

Fig. 1. SRIM calculated damage profiles in the units of displacement per atom (dpa) generated by 3 MeV Fe ions for the Fe-1.0 at% Cu alloy. Similar radiation damage levels are calculated to the Fe-Au alloy.

of 550 °C. Self-ions irradiation is an efficient method to simulate neutron irradiation effects. When the Fe ions penetrate the material, they are slowed down primarily by the electronic energy loss. Meanwhile, they can interact with the sample atoms via nuclear collisions. Defects are induced in the cascade of atoms. The depth dependent radiation damage (expressed in units of the displacement per atom, dpa) is shown in Fig. 1, simulated by the Stopping and Range of Ions in Matter (SRIM) software [24]. The calculation is based on the Kinchin–Pease mode and the Fe-displacement energy is set to be 40 eV [25,26]. At a fluence of 2.66×10^{15} ions/cm^2, the corresponding irradiation damage peak dose is 2.8 dpa at a depth of 840 nm for Fe-1.0 at% Cu alloy. At a fluence of 7.98×10^{15} ions/cm^2, the corresponding irradiation damage peak dose is 8.3 dpa at the same depth. The damage rate was 1.3×10^{-4} dpa/s. The microstructures after irradiation were examined by transmission electron microscopy (TEM) using a Tecnai G2 F20ST/STEM instrument operating at 200 keV. The TEM sample preparation technique is as follows: the sample was adhered with M−bond 610 and biaxially grounded to a thickness < 20 μm. Afterwards, an ion beam thinner (Gatan691) was used to obtain electron transparency with Ar ions at room temperature. The voltage decreased from 4.8 kV to 3.2 kV corresponding to the incidence angle from 10° to 4°.

Nano-indentation tests (Nano indenter G200, Agilent) were performed using continuous stiffness measurement method with a diamond Berkovich tip. At least five indents with a spacing between indents of 50 μm and an indentation depth up to 1200 nm were measured per condition. The hardness-depth curves were analyzed with the method developed by Oliver and Pharr [27].

3. Results and discussion

Fig. 2 shows the the cross-section TEM micrographs for the Fe-Au alloy after self-ion irradiation to a level of 2.8 dpa, indicating the formation of damage and precipitates. Close to the surface, a high density of thin-plate-like precipitates was observed, as shown in Fig. 2b. At higher implantation depths, dislocations were generated. High magnification images for the maximum damage region (Fig. 2c) and a region in a depth of around 1100 nm (Fig. 2d) indicate that all observed dislocations were decorated by thin plates, suggesting a causal connection between precipitates and the presence of radiation damage. A HAADF mode micrograph is shown in Fig. 2f with the corresponding Au elemental map (Fig. 2g). TEM micrographs (Fig. 2e, f) indicate that the thin plates were disc-shape Au-rich precipitates, consistent with previously reported results on the precipitate structure in cold-deformed Fe-Au alloys after aging [28]. It is worthy mentioning that the

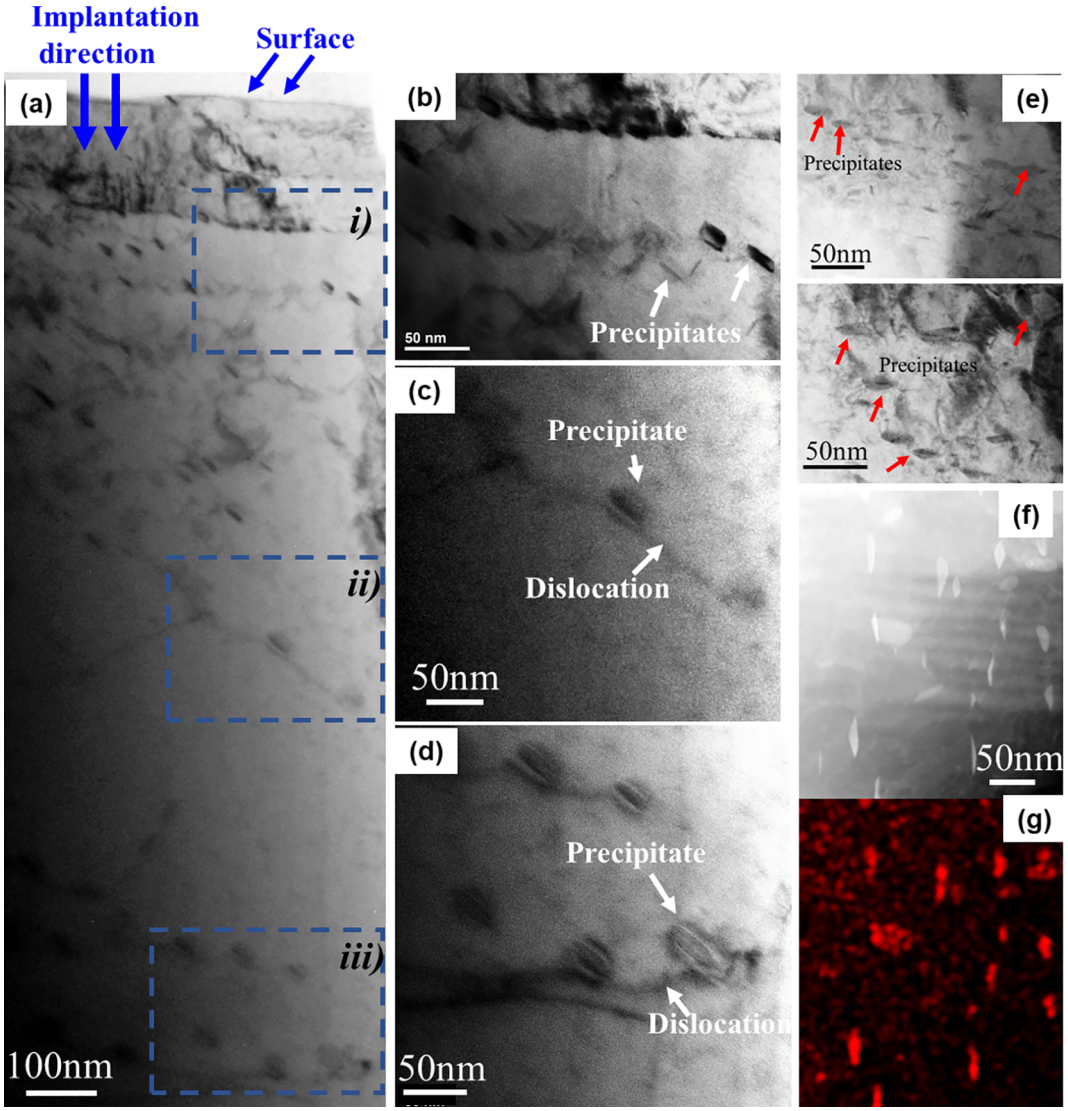

Fig. 2. (a–e) Bright Field TEM for the Fe-Au sample after Fe-ion irradiation to a level of 2.8 dpa; (b, c, d) are high magnification images for the regions labelled as i, ii, iii in (a), respectively. (f) HAADF mode image with corresponding Au elemental mapping (g).

correlation between Au precipitates and the dislocations matches well with the mechanism that Au precipitates are nucleated exclusively on dislocations as proposed by Hornbogen [19]. The segregation and precipitation of Au atoms on the dislocations play a role in dislocation pinning. The site-specific heterogeneous nucleation of Au precipitates on dislocations is the result of the strongly reduced nucleation activation barrier due to the local change in surface and strain energy.

The microstructure of the Fe-Cu alloy after an irradiation dose of 2.8 dpa is shown in Fig. 3. Radiation damage manifests itself in the form of dislocations and dislocations loops (Fig. 3a–d). A HAADF mode micrograph with the corresponding Cu elemental map indicated the formation of a high density of nanoscale Cu precipitates with spherical shape, as shown in Fig. 3e and f. Most nano-size Cu precipitates were homogeneously formed in the Fe matrix at locations without detectable radiation damage. In contrast to the Fe-Au alloy sample, no spatial correlation between the Cu precipitates and radiation damage could be established in the Fe-Cu alloy.

It is well known that positrons are a sensitive probe for vacancy-type defects in the iron matrix. Moreover, positrons are trapped differently by embedded ultrafine particles, like Cu clusters/precipitates [10,29] or Au precipitates [30]. The *S* parameter represents the fraction of positron annihilations as a result of interactions with low momentum electrons and the value of the parameter increases for an increasing concentration of vacancy-type defects. The *W* parameter reflects the fraction of positron annihilation with high momentum electrons. The annihilation of positrons with the Au-rich and Cu-rich clusters will cause an increase in the selected high-momentum regions, resulting in higher values for the *W* parameter. Moreover, the evolution of the *S* and *W* parameters with incident positron energy can provide information on the solute–vacancy complexes [31]. Fig. 4 shows the evolution of the *S* and *W* parameters with increasing incident positron energy for the irradiated Fe-Au and the Fe-Cu alloys as well as the data for the samples in their unirradiated state. For the Fe-Au alloy, the *S* parameters increased significantly for a dose of 2.8 dpa in comparison to the unirradiated sample, signalling the formation of open volume defects. The *S* parameter values decreased when the irradiation dose was increased to a dose of 8.3 dpa. It is mainly due to i) the increase of the *W* parameters after 8.3 dpa and ii) the Au precipitation at dislocations. A peak appeared in the *S(E)* curve in the positron energy range from around 4 to 14 keV for the sample with a dose of 8.3 dpa, which may result from the migration and aggregation of defects considering the long-term irradiation (18 h) at high temperature (550 °C) [32]. For the Fe-Cu, the S (E) curves for the unirradiated sample is close to that of the unirradiated Fe-Au alloy sample. The *S* parameters for the irradiated

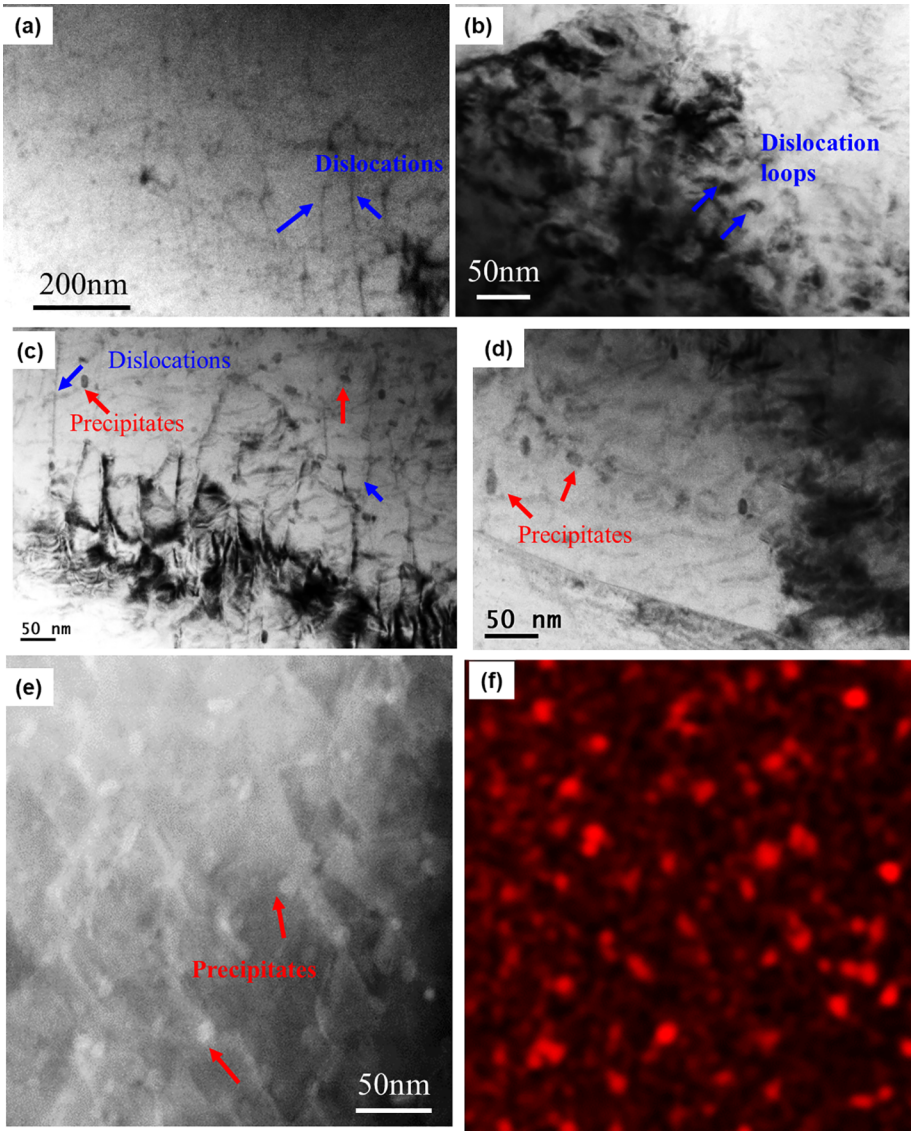

Fig. 3. (a–d) Bright Field TEM for the Fe-Cu sample after Fe-ion irradiation to a level of 2.8 dpa, (e) HAADF mode image with corresponding Cu elemental mapping (f).

samples were higher than those for the unirradiated sample and the *S* parameters increased with the irradiation dose. Similar to the Fe-Au alloy, for the Fe-Cu alloy irradiated with a dose of 8.3 dpa a defect peak was observed.

The difference of the *W(E)* curves was negligible for the unirradiated Fe-Au and Fe-Cu alloy samples. A decrease in the *W* parameters was observed for the irradiated Fe-Au alloy samples compared to the unirradiated sample. Since the *S* and *W* values are the result of a competition of annihilation in different states [10], the decrease of the *W* parameters primarily arises from the increase of the *S* parameters. For the Fe-Cu, the annihilation of positrons with Cu precipitates/clusters contributed significantly to the increase of the *W* parameters upon irradiation.

Fig. 5 shows the *S* versus *W* plots for the Fe-Au and Fe-Cu alloy samples. The *S*–*W* plots reflect the energy-dependent evolution of the open volume defects and their chemical environment. The (*S, W*) points for the unirradiated Fe-Au and Fe-Cu followed a single linear relationship (labelled as L_0): *S* decreased and *W* increased with increasing positron energy. After irradiation, the *S*-*W* plots of the Fe-Au alloy followed a similar linear relationship as that of the unirradiated sample. It suggested that positrons were trapped by the open volume defects and annihilated with the free electrons in the Fe matrix. Based on the SRIM calculations (Fig. 1) and the TEM measurements (Fig. 2), radiation damage, in the form of dislocations, was generated by implantation of 3 MeV Fe ions. Moreover, our previous study revealed that a mixture of dislocations and vacancy-type misfit were formed between the Au precipitates and the Fe matrix [30]. Those open volume defects acted as the dominate trapping sites for the positrons. On the contrary, the *S*-*W* plots for the irradiated Fe-Cu deviated from the single straight line. The evolution of the (*S*, *W*) points was divided into two segments. Region I and II correspond to a positron energy range of 0.5–8 keV and 8–25 keV, respectively. Based on the experimental and theoretical results from Jin and coworkers where self-ions with a similar energy were implanted [11], Cu precipitates and Cu_nV_m complexes ($n > m$) are expected to be the dominant microstructure features in the region I whereas open volume defects, in the forms of dislocations and dislocation loops and Cu_nV_m complexes ($n < m$) are the main defect types in the region II.

The indentation-depth dependence of hardness of the Fe-Au and Fe-Cu alloys at different levels of irradiation is shown in Fig. 6a. The hardness values *H* of the unirradiated Fe–Au alloy are obviously higher than those of the unirradiated Fe-Cu alloy. It is attributed to the larger

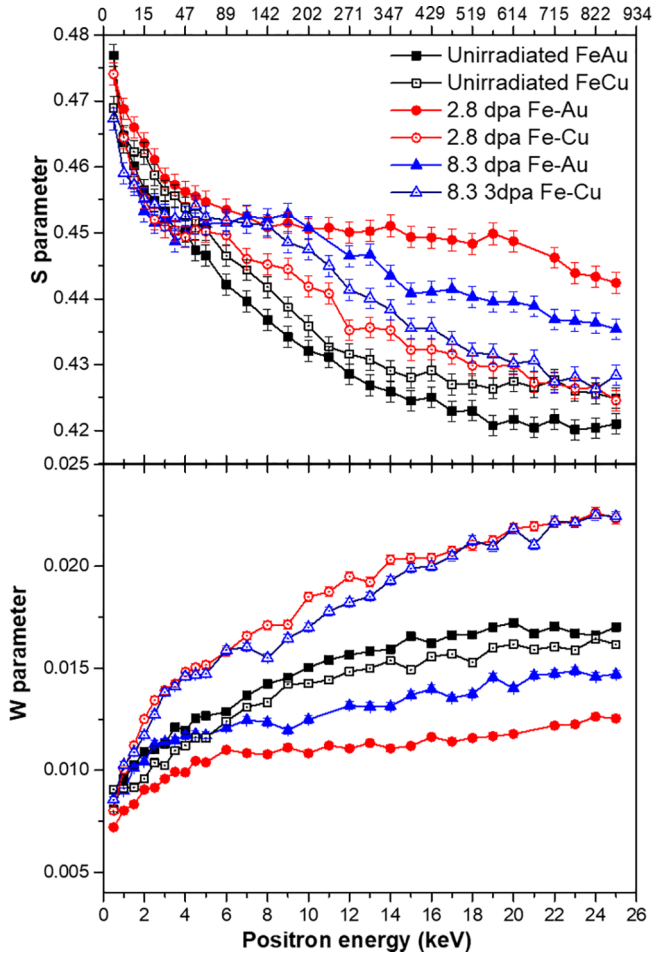

Fig. 4. (a) *S(E)* curves and (b) *W(E)* curves for Fe-Au and Fe-Cu alloy samples unirradiated and irradiated with a dose of 2.8 and 8.3 dpa, respectively.

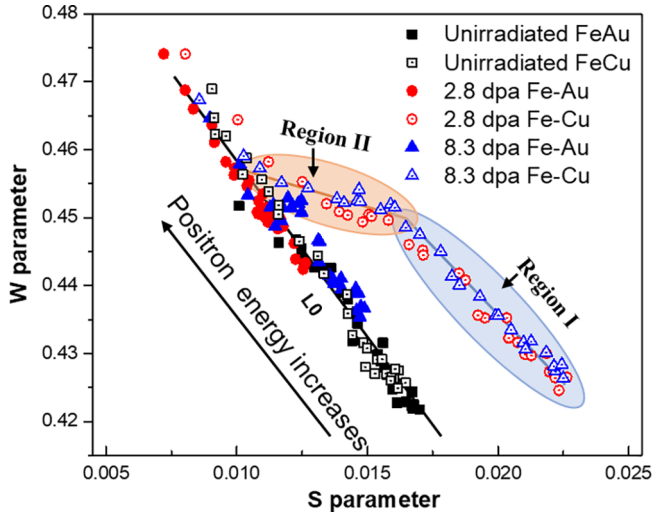

Fig. 5. *S-W* plots for the unirradiated and irradiated Fe-Au and Fe-Cu alloy samples.

atomic size factor for solute Au [23], which generates a higher local strain field, resulting in an enhanced strain hardening. A significant irradiation-induced hardness increase was observed for the Fe-Au alloy at a dose of 2.8 dpa while the hardness slightly decreased when the irradiation dose was increased to 8.3 dpa. In contrast, for the Fe-Cu alloy a slight hardening was observed at an irradiation dose of 2.8 dpa

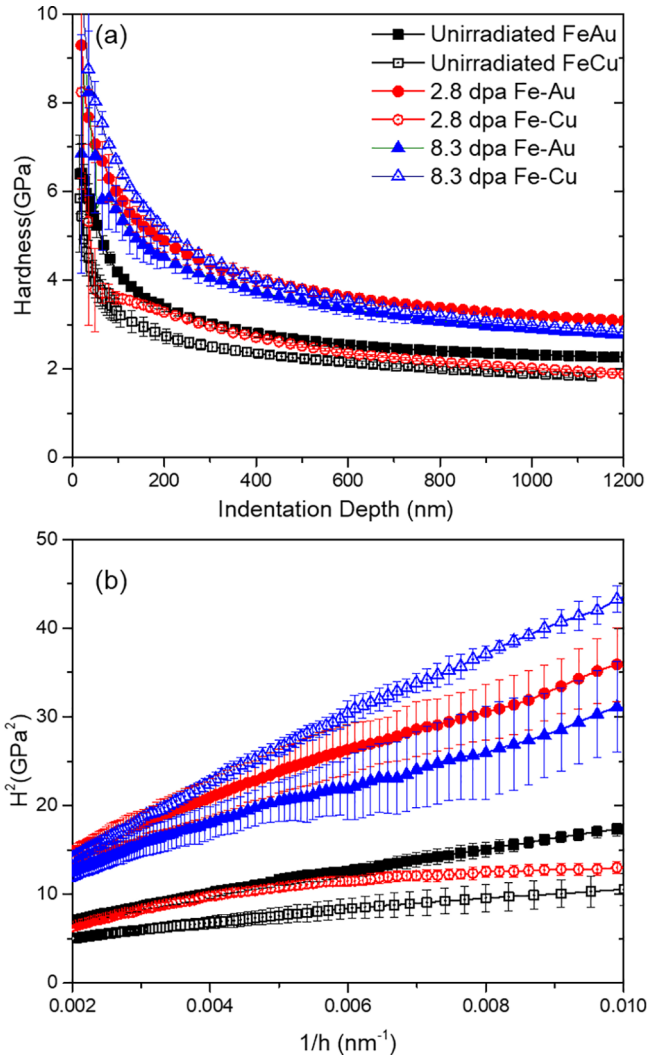

Fig. 6. (a) Dependence of hardness H on depth h and (b) the dependence of H^2 on $1/h$ for the Fe-Au and Fe-Cu alloys at different irradiation dose levels. The same symbol characterisation applies to both figures.

followed by a large increase in hardness at an irradiation dose of 8.3 dpa.

For all samples, the hardness decreased with increasing penetration depth, a feature which is known as the indentation size effect (ISE). Nix and Gao developed a model based on the geometrically necessary dislocation (GND) theory to explain the size effect [33]. The nanoindentation hardness-depth formula can be described as follows:

$$\frac{H}{H_0} = \sqrt{1 + \frac{h^*}{h}} \tag{1}$$

where H is the hardness at a given depth h; H_0 is the hardness at infinite depth, $h^*$is a characteristic length depending on the shape of the indenter, the shear modulus and H_0. The hardness data are plotted as H^2 versus $1/h$ in Fig. 6(b).

The square of the nanoindentation hardness is proportional to the reciprocal of indentation depth, which is consistent with the description in Eq. (1). H_0 was calculated by the least square fitting of hardness within the depth of $100 < h < 500$ nm where the plastic zone of the indent had not extended beyond the damage layer into the unirradiated bulk [34,35]. The values of H_0 were the real hardness of the materials weakening the indentation size effects and are considered as the macroscopic hardness [36,37]. The values of H_0 for the Fe-Au and Fe-Cu alloy samples were summarized in Table. 2 and the evolution of the

Table 2
Hardness (H_0) of Fe-Au and Fe-Cu alloy samples at different irradiation levels.

Irradiation dose (dpa)	Fe-Au		Fe-Cu	
	H_0	ΔH_0	H_0	ΔH_0
0	2.15	0	1.94	0
2.8	3.14	0.99	2.32	0.38
8.3	2.96	0.81	2.66	0.72

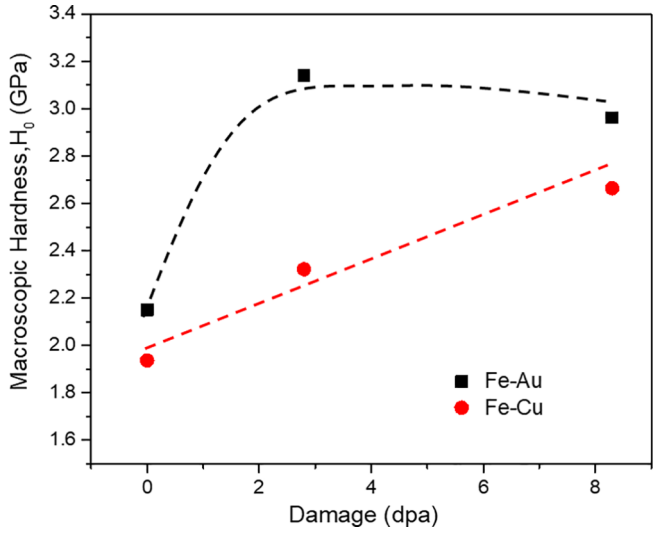

Fig. 7. Comparison of the irradiation hardening of the Fe-Au and Fe-Cu.

hardness with the irradiation for both alloys was shown in Fig. 7. The macroscopic hardness of the as-quenched Fe-Cu is 1.94 GPa, which is close to the reported value [18]. Radiation hardening was observed for the Fe-Cu alloy samples, due to the formation of dislocations, dislocations loops and precipitates (as indicated in Figs. 2 and 3). The Cu precipitates were reported to be inherited from {0 1 1} Fe planes [38]. The possible slip planes for the bcc Fe and Fe-based alloys also include {1 1 0} planes [39]. It implies the pining effects of the Cu precipitates on the slipping of the dislocations. The hardening increased with the irradiation dose. The macroscopic hardness for the as-quenched Fe-Au alloy was higher than that of the as-quenched Fe-Cu alloy. The Fe-Au alloy hardened dramatically after a dose of 2.8 dpa, which was attributed to the enhanced strain hardening due to the irradiation-induced dislocations and Au-rich clusters and precipitates. In contrast to the Fe-Cu alloy, the hardening behaviour for the Fe-Au alloy was slightly inhibited as the dose was increased from 2.8 to 8.3 dpa. It may arise from the recovery and migration of irradiation-induced defects [17], as supported by the VEPAS results (in Fig. 4). Moreover, the interaction of solute Au atoms with dislocations is expected to increase with the high irradiation time, resulting in a reduction of the strain fields of dislocations and substitutionally dissolved Au atoms, i.e. to a lowering of the degree of strain hardening.

4. Conclusions

Fe-1at.%Au and Fe-1at.%Cu alloys are irradiated with Fe self-ions at 550 ˚C to simulate the service condition in a nuclear reactor and to investigate the correlation between radiation damage and Au/Cu precipitation. For the irradiated Fe-Au alloy, an increase in the *S* parameters upon irradiation indicates the formation of open volume defects. The *S-W* plots suggest a similar positron annihilation mechanism for the irradiated samples as for the unirradiated sample. A close interaction between the Au precipitates and the radiation induced dislocations, which is absent in the irradiated Fe-Cu materials, is observed in the TEM micrographs. For the Fe-Cu alloy, the increase in the *S* and *W* parameters in VEPAS corresponds to the formation of radiation damage and Cu precipitates, respectively. The irradiation-induced defects show a significantly different behavior is two regions. Radiation hardening is observed for both alloys. As the irradiation dose increases, the hardness shows a negligible enhancement for the Fe-Au alloy while the hardness continues to increase for the Fe-Cu alloy.

CRediT authorship contribution statement

Shasha Zhang: Conceptualization, Investigation, Writing - original draft, Funding acquisition. **Zhengjun Yao:** Project administration. **Zhaokuan Zhang:** Data curation, Investigation. **Moliar Oleksandr:** Supervision. **Feida Chen:** Formal analysis. **Xingzhong Cao:** Methodology. **Peng Zhang:** Data curation. **Niels van Dijk:** Writing - review & editing. **Sybrand van der Zwaag:** Conceptualization, Writing - review & editing.

Declaration of Competing Interest

The authors declare that they have no known competing financial interests or personal relationships that could have appeared to influence the work reported in this paper.

Acknowledgements

This research was supported by the Natural Science Foundation of Jiangsu Province, China (Grant No. BK20170798), the National Natural Science Foundation of China (Grant No. 51701095). We appreciated the support of highly charged ions on the 320 kV-platform at the institute of Modern Physics, CAS.

References

[1] S.J. Zinkle, G.S. Was, Materials challenges in nuclear energy, Acta Mater. 61 (2013) 735–758.
[2] T. Allen, J. Busby, M. Meyer, D. Petti, Materials challenges for nuclear systems, Mater. Today 13 (2010) 14–23.
[3] R.A. Johnson, N.Q. Lam, Solute segregation in metals under irradiation, Phys. Rev. B 13 (1976) 4364–4375.
[4] N.Q. Lam, P.R. Okamoto, H. Wiedersich, Effects of solute segregation and precipitation on void swelling in irradiated alloys, J. Nucl. Mater. 74 (1978) 101–113.
[5] S. Jin, L. Guo, F. Luo, Z. Yao, S. Ma, R. Tang, Ion irradiation-induced precipitation of Cr23C6 at dislocation loops in austenitic steel, Scr. Mater. 68 (2013) 138–141.
[6] K. Ono, K. Arakawa, K. Hojou, Formation and migration of helium bubbles in Fe and Fe–9Cr ferritic alloy, J. Nucl. Mater. 307 (2002) 1507–1512.
[7] J. Yan, Z. Tian, W. Xiao, W. Geng, Interaction of He with Cu, V, and Ta in bcc Fe: A first-principles study, J. Appl. Phys. 110 (2011) 013508-1–6.
[8] F. Soisson, C.C. Fu, Cu-precipitation kinetics in α − Fe from atomistic simulations: vacancy-trapping effects and cu-cluster mobility, Phys. Rev. B 76 (2007) 214102-1–12.
[9] G. Odette, B. Wirth, A computational microscopy study of nanostructural evolution in irradiated pressure vessel steels, J. Nucl. Mater. 251 (1997) 157–171.
[10] S. Jin, P. Zhang, E. Lu, L. Guo, B. Wang, X. Cao, Correlation between Cu precipitates and irradiation defects in Fe–Cu model alloys investigated by positron annihilation spectroscopy, Acta Mater. 103 (2016) 658–664.
[11] S. Jin, X. Lian, T. Zhu, Y. Gong, P. Zhang, X. Cao, R. Yu, B. Wang, Irradiation evolution of Cu precipitates in Fe1.0Cu alloy studied by positron annihilation spectroscopy, J. Nucl. Mater. 499 (2018) 65–70.
[12] Q. Xu, T. Yoshiie, K. Sato, Dose dependence of Cu precipitate formation in Fe − Cu model alloys irradiated with fission neutrons, Phys. Rev. B 73 (2006) 134115-1–6.
[13] G. Was, M. Hash, R. Odette, Hardening and microstructure evolution in proton-irradiated model and commercial pressure-vessel steels, Phil. Mag. 85 (2005) 703–722.
[14] Y. Nagai, Z. Tang, M. Hassegawa, T. Kanai, M. Saneyasu, Irradiation-induced Cu aggregations in Fe: an origin of embrittlement of reactor pressure vessel steels, Phys. Rev. B 63 (2001) 134110-1–5.
[15] R. Wang, C. Xu, X. Liu, P. Huang, A. Ren, Microstructural and mechanical studies of reactor pressure vessel steel under proton irradiation, J. Alloys Comp. 581 (2013) 788–792.
[16] R. Wang, X. Liu, A. Ren, J. Jiang, C. Xu, P. Huang, Y. Wu, C. Zhang, X. Wang, Proton-irradiation-induced damage in Fe–0.3 wt.% Cu alloys characterized by positron annihilation and nanoindentation, Nucl. Instrum. Methods Phys. Res., Sect. B 307 (2013) 545–551.
[17] C.D. Hardie, C.A. Williams, S. Xu, S.G. Roberts, Effects of irradiation temperature and dose rate on the mechanical properties of self-ion implanted Fe and Fe–Cr

alloys, J. Nucl. Mater. 439 (2013) 33–40.
[18] K. Yabuuchi, H. Yano, R. Kasada, H. Kishimoto, A. Kimura, Dose dependence of irradiation hardening of binary ferritic alloys irradiated with Fe3+ ions, J. Nucl. Mater. 417 (2011) 988–991.
[19] E. Hornbogen, The role of strain energy during precipitation of copper and gold from alpha iron, Acta Metall. 10 (1962) 525–533.
[20] W. Hao, W. Geng, Gold might slow down the growth of helium bubble in iron, Nucl. Instrum. Methods Phys. Res., Sect. B 269 (2011) 1428–1430.
[21] T. Ohnuma, N. Soneda, M. Iwasawa, First-principles calculations of vacancy–solute element interactions in body-centered cubic iron, Acta Mater. 57 (2009) 5947–5955.
[22] S. Zhang, J. Cizek, Z.J. Yao, M. Oleksandr, X.S. Kong, C.S. Liu, N. van Dijk, S. van der Zwaag, Self healing of radiation-induced damage in Fe–Au and Fe–Cu alloys: Combining positron annihilation spectroscopy with TEM and ab initio calculations, J. Alloy. Compd. (2019, In Press).
[23] H. King, Quantitative size-factors for metallic solid solutions, J. Mater. Sci. 1 (1966) 79–90.
[24] J.F. Ziegler, M.D. Ziegler, J.P. Biersack, SRIM–The stopping and range of ions in matter, Nucl. Instrum. Methods Phys. Res., Sect. B 268 (2010) 1818–1823.
[25] R.E. Stoller, M.B. Toloczko, G.S. Was, A.G. Certain, S. Dwaraknath, F.A. Garner, On the use of SRIM for computing radiation damage exposure, Nucl. Instrum. Methods Phys. Res., Sect. B 310 (2013) 75–80.
[26] J. Hunn, E. Lee, T. Byun, L. Mansur, Ion-irradiation-induced hardening in Inconel 718, J. Nucl. Mater. 296 (2001) 203–209.
[27] W.C. Oliver, G.M. Pharr, An improved technique for determining hardness and elastic modulus using load and displacement sensing indentation experiments, J. Nucl. Mater. 7 (1992) 1564–1583.
[28] S. Zhang, J. Kohlbrecher, F. Tichelaar, G. Langelaan, E. Brück, S. van der Zwaag, N. van Dijk, Defect-induced Au precipitation in Fe–Au and Fe–Au–B–N alloys studied by in situ small-angle neutron scattering, Acta Mater. 61 (2013) 7009–7019.
[29] Y. Nagai, M. Hasegawa, Z. Tang, A. Hempel, K. Yubuta, T. Shimamura, Y. Kawazoe, A. Kawai, F. Kano, Positron confinement in ultrafine embedded particles: quantum-dot-like state in an Fe-Cu alloy, Phys. Rev. B 61 (2000) 6574–6578.
[30] S. Zhang, H. Schut, J. Čížek, F. Tichelaar, E. Brück, S. van der Zwaag, N. van Dijk, Positron annihilation study on deformation-induced Au precipitation in Fe–Au and Fe–Au–B–N alloys, J. Mater. Sci. 49 (2014) 2509–2518.
[31] A. Somoza, M. Petkov, K. Lynn, A. Dupasquier, Stability of vacancies during solute clustering in Al-Cu-based alloys, Phys. Rev. B 65 (2002) 094107-1–6.
[32] P. Zhang, S. Jin, E. Lu, B. Wang, Y. Zheng, D. Yuan, X. Cao, Effect of annealing on VmHn complexes in hydrogen ion irradiated Fe and Fe–0.3% Cu alloys, J. Nucl. Mater. 459 (2015) 301–305.
[33] W.D. Nix, H. Gao, Indentation size effects in crystalline materials: A law for strain gradient plasticity, J. Mech. Phys. Solids 46 (1998) 411–425.
[34] C.D. Hardie, S.G. Roberts, Nanoindentation of model Fe–Cr alloys with self-ion irradiation, J. Nucl. Mater. 433 (2013) 174–179.
[35] K. Yabuuchi, R. Kasada, A. Kimura, Effect of alloying elements on irradiation hardening behavior and microstructure evolution in BCC Fe, J. Nucl. Mater. 442 (2013) S790–S795.
[36] Z. Fu, P. Liu, F. Wan, Q. Zhan, Helium and hydrogen irradiation induced hardening in CLAM steel, Fusion Eng. Des. 91 (2015) 73–78.
[37] D. Zhao, S. Li, Y. Wang, F. Liu, X. Wang, Investigation of ion irradiation hardening behaviors of tempered and long-term thermal aged T92 steel, J. Nucl. Mater. 511 (2018) 191–199.
[38] P.J. Othen, M.L. Jenkins, G.D.W. Smith, High-resolution electron microscopy studies of the structure of Cu precipitates in α-Fe, Philoso. Mag. 70 (1994) 1–23.
[39] C.R. Weinberger, B.L. Boyce, C.C. Battaile, Slip planes in bcc transition metals, Int. Mater. Rev. 5 (2013) 296–314.